

Journal of Materials Chemistry A

Accepted Manuscript



This is an *Accepted Manuscript*, which has been through the Royal Society of Chemistry peer review process and has been accepted for publication.

Accepted Manuscripts are published online shortly after acceptance, before technical editing, formatting and proof reading. Using this free service, authors can make their results available to the community, in citable form, before we publish the edited article. We will replace this *Accepted Manuscript* with the edited and formatted *Advance Article* as soon as it is available.

You can find more information about *Accepted Manuscripts* in the [Information for Authors](#).

Please note that technical editing may introduce minor changes to the text and/or graphics, which may alter content. The journal's standard [Terms & Conditions](#) and the [Ethical guidelines](#) still apply. In no event shall the Royal Society of Chemistry be held responsible for any errors or omissions in this *Accepted Manuscript* or any consequences arising from the use of any information it contains.

Cite this: DOI: 10.1039/c0xx00000x

www.rsc.org/xxxxxx

Site Specific Supramolecular Heterogeneous Catalysis by Optically Patterned Soft Oxometalate - Porous Organic Framework (SOM-POF) Hybrid on a Chip

Preethi Thomas^a, Cuiying Pei^b, Basudev Roy^c, Subhrokoli Ghosh^c, Santu Das^a, Ayan Banerjee^{c*}, Teng Ben^{b*}, Shilun Qiu^b and Soumyajit Roy^{a*}

Received (in XXX, XXX) Xth XXXXXXXXX 20XX, Accepted Xth XXXXXXXXX 20XX

DOI: 10.1039/b000000x

We have designed a supramolecularly bound multi-component catalytic material based on a soft oxometalate (SOM) and a porous organic framework (POF) material which shows high catalytic conversion efficiency. We have also used this material for site directed supramolecular heterogeneous catalysis with yield even higher than in the bulk, and with micron-level precision by controllably depositing the material on a glass substrate, making a reactor chip, using a thermo-optical tweezers. Various SOM-POF composites have been prepared in dispersion phase and patterned using thermo-optic tweezers and their catalytic activities have been compared with a benchmark molecular catalyst [PMo₁₂]. This work can lead to further explorations for hybrid materials formed out of well defined molecular level precursors which can be controllably micro-patterned in order to catalyze targeted reactions simultaneously.

Introduction

An immediate challenge in supramolecular catalysis is to design high surface area supramolecularly bound multi-component catalytic materials in a controlled fashion. In such a design it is desired that distinct multifunctional components are held together by supramolecular interactions and they function catalytically in synergy to emulate enzymes.¹ Moreover for efficient catalysis high surface area materials are required.

Hence the need of the hour for supramolecular catalysis¹ translates to the following questions. Is it possible to bring multiple functional components together? Can they be held together such that they can act in synergy? Can these components be patterned as ultrahigh surface area materials that show catalytic activities? Here in this paper we address these challenges simultaneously. We start with a soft oxometalate, (SOM) dispersion² of molybdenum containing nanotubes to which we add porous organic framework (POF) material, to get a stable soft oxometalate-porous organic framework, (SOM-POF) dispersion. We then expose this dispersion to a thermo-optic laser tweezers to induce a phase transition from a dispersion to a crystalline state – thereby simultaneously patterning³⁻¹¹ the material in solid state by translating the laser beam.¹² We further use this patterned material to carry out site-directed supramolecular catalysis.^{13, 14} It is perhaps now apt to introduce the components of this material and the physical techniques we use separately and briefly.

Soft oxometalates or SOMs are oxometalates endowed with soft matter properties² of transition metal-oxide clusters known as polyoxometalates (POMs).^{15,16} POMs have been extensively studied owing to their potential applications in various fields such as catalysis, electrical conductivity, sensing, medicinal chemistry and material science.¹⁶⁻³¹ SOMs are primarily governed by non-covalent interactions and can be moved with precision in an optical field^{2a} and they show topological transformation.^{2e} Soft oxometalates have large surface areas which can be easily manipulated and exploited in catalysis. In this work we use

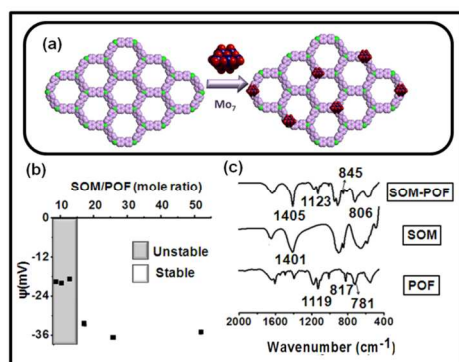


Fig. 1 (a) Schematic representation of ammonium heptamolybdate tetrahydrate (red-blue clusters) soft oxometalate incorporated into JUC-Z4 (Phosphorous represented in green colour) porous organic framework. (b) Ψ , Zeta potential of various SOM-POF dispersions versus SOM/POF (mole ratio). (c) FTIR Spectra of SOM-POF composite catalyst showing shifts in the N-H (1405 cm⁻¹) and C-H (845 cm⁻¹) bending frequencies and C-H (806 cm⁻¹) and C-P (1123 cm⁻¹) stretching frequencies.

ammonium heptamolybdate tetrahydrate as the crystalline precursor to soft oxomolybdate.

The second component used in our work is POF or porous organic framework. POFs are porous materials³² with high surface area per unit mass as compared to metal-organic frameworks³³ and are extremely stable chemically as well as thermally. These materials provide accessible space within their pores for reactant molecules to react.³⁴⁻⁴⁰ Such porous frameworks are hence known for their applications in gas storage⁴¹⁻⁴⁶ and separation⁴⁷. These porous frameworks are known to have affinity towards greenhouse gases such as carbon dioxide, methane, and exhibit high selectivity towards them in gas sorption studies.^{48a} While SOMs provide catalytic potential, POFs provide high surface area and accessible space within the framework when these two components are combined together. JUC-Z4 used in this work is an electroactive porous organic framework synthesized from tris(4-chlorophenyl)phosphine, in which the radical redox centre of phosphorous is stabilized by an aromatic organic framework. The pore size, BET surface area and polarity of these organic frameworks can be manipulated and controlled by redox reactions.^{48a} Furthermore we also synthesized composites using other POF materials such as PAF1, JUC-Z2 and JUC-Z5 to form SOM-PAF1, SOM-JUC-Z2, SOM-JUC-Z5 composites respectively. PAF1 is an extensively studied POF with exceptionally high surface area and thermal stability. It has a diamondoid structure with a tetrahedral carbon surrounded by phenyl rings. JUC-Z2 is similar to JUC-Z4 except for the hetero atom in this porous material is nitrogen instead of phosphorous. JUC-Z5 on the other hand is the oxidised form of JUC-Z4 with phosphorous in the +5 oxidation state.⁴⁸

It is the redox activity of JUC-Z4 coupled with the presence of phosphorous in it that prompted us to ask the following questions. Phosphomolybdates are known to be catalysts for several reactions.^{18, 49} Can a supramolecular composite in dispersion state comprising of both molybdenum and phosphorous show comparable catalytic property as that of [PMo₁₂] Keggin? Can the catalytic activity of such a SOM-POF composite (SOM-JUC-Z4) be compared with other SOM-POF composites? Can we furthermore design high surface area patterned surfaces starting from such SOM-POF supramolecular composite dispersion? In addition to addressing these questions we further compare and contrast the catalytic activity of SOM-POF composites in dispersions. We demonstrate the catalytic activity of various thermo-optically patterned composite SOM-POF catalyst chips. We show the stability of such catalytic chips before and after reaction and over days. We ask: can both aliphatic and aromatic aldehydes be oxidized by our method? Can other oxidants be used? How efficient is our SOM-POF chip compared to that of [PMo₁₂] benchmark catalyst?

Materials and Methods

Ammonium heptamolybdate tetrahydrate is used as obtained. JUC-Z4 is prepared following the previously published procedure.⁴⁸ Benzaldehyde, hydrogen peroxide and DMSO were used as obtained. All chemicals are obtained from Merck.

Synthesis of SOMs

1.236 g (0.001 moles) of ammonium heptamolybdate tetrahydrate is dissolved in 10 mL of distilled water to prepare 0.1 M solution. Then 0.2 M solution is prepared by dissolving 2.472 g (0.002 moles) of the heptamolybdate in 10 mL of distilled water. The two solutions of 0.1 M and 0.2 M are then warmed until dispersions are obtained that scatter laser light. These SOM dispersions were refrigerated for about 10 minutes for further experiments.

Preparation of SOM-POF dispersions

Mole ratios of SOM and JUC-Z4 dispersions are varied from 1.3:1 to 51.8:1 (SOM:JUC-Z4) and 10 colloidal dispersions of SOM-POF hybrids are prepared. The same procedure is followed to prepare dispersions of SOM-PAF1, SOM-JUC-Z2 and SOM-JUC-Z5.

Description of Optical Tweezers set up

The optical patterning is done exactly similar to the procedure adopted in our previous work.¹² The SOM-POF dispersion is patterned by exposing it to thermo-optical tweezers. The dispersion is placed between a 1 mm thick standard glass slide (top surface) and a 160 μm thick glass cover-slip (bottom surface). The spacing between the two surfaces is controlled by putting double-sided sticky tape on the sides of the cover-slip. This set-up of slide and cover-slip stuck together with double-sided sticky tape constitute the sample holder. The dispersion in this holder is impinged with a CW laser beam which is focused to a diffraction limited spot by a high numerical aperture objective lens. The thermo-optical tweezers set up is built around an inverted microscope (Zeiss Axiovert. A1Observer), and it has a 100X, 1.4 N.A. oil immersion microscope objective (Zeiss planoapochromat, infinity corrected) which is used to focus light from a diode laser (Lasever LSR1064ML) of 1064 nm wavelength on the sample holder to attain a spot size of waist radius ~ 500 nm. The power of the laser can be varied from 0 to 100 mW after the objective. Before every experimental run, the slide and coverslip constituting the sample holder are rinsed with methanol and dried in order to remove the presence of any adsorbed impurity. The sample holder containing about 75 μL of the dispersion is translated using the microscope scanning stage which is stepper motor controlled with a Ludl MAC5000 XY stage controller operated by a joystick. The total travel range of the stage is 130 x 100 mm with a resolution of 100 nm. The patterning process is observed on a monitor with the help of a CCD camera (Axiovision) running at a fastest rate of 30 frames per second. A combination of 10X/40X/100X objectives and external optics are arranged outside the microscope to aid in imaging which is done at the back focal part of microscope.

Zeta Potential Measurements

Malvern Zetasizer instrument coupled with Malvern Zetasizer software is used to measure zeta potential of prepared SOM-POF dispersions in folded capillary cell.

FTIR Spectroscopy

Perkin Elmer Spectrum RX1 spectrophotometer is used to record the FTIR spectra in the range of 400-4000 cm^{-1} .

Low pressure N_2 adsorption measurements

N_2 sorption isotherm measurements were performed with a Micromeritics Tristar II 3020 surface area and pore size analyser. Before the measurement, the sample was subjected to a degas vacuum system under ultra high vacuum (90mtorr) at 100°C for 12 h. The sample was backfilled with nitrogen and transferred to the analysis system. A sample of 50mg and ultra high purity grade nitrogen (99.999%) gas source were used in the nitrogen sorption measurements at 77 K, maintained with liquid nitrogen throughout the measurement. Helium was used for the free space determination after sorption analysis, both at ambient temperature and at 77K. Apparent surface areas were calculated from nitrogen adsorption data by multi-point Brunauer–Emmett–Teller (BET) analysis. Apparent micropore distributions were calculated from carbon dioxide adsorption data by the density functional theory (DFT) method.

Thermogravimetric Analysis

The TGA was performed using a Shimadzu DTG-60 thermal analyser system at a heating rate of 10°C min^{-1} to 800°C in a dried air atmosphere and the air flow rate was 30ml min^{-1} . The sample was loaded in an alumina pan.

Raman Spectroscopy

A LABRAM HR800 Raman spectrometer is employed using the 633 nm line of a He-Ne ion laser as the excitation source to analyze the sample.

Transmission Electron Microscopy

The characterization of the composite was primarily done by the use of a Tecnai 20 transmission electron microscope (FEI Company) operated at an accelerating voltage of 200 kV. The TEM micrographs have been processed using SIS software (Soft Imaging System).

Nuclear Magnetic Resonance

Time dependent ^1H NMR measurements were performed using 400 MHz Bruker Ultrashield Plus System.

Results and Discussion

1. On formation of SOM-POF composites and their characterization:

We first analyze the formation of the supramolecular composite between molybdenum containing soft oxometalate and the phosphorous containing porous organic framework. To do so, we first need to check whether a stable dispersion can be obtained using soft oxometalates and porous organic frameworks in synergy. We now check systematically what happens when a

SOM dispersion is mixed with a phosphorous containing POF (JUC-Z4). Upon mixing, we get a colloidal dispersion of SOM-POF composite. The colloidal nature of such stable dispersions is confirmed by passing laser light through these dispersions and checking for the scattering of light. We further see that as we vary the relative loading of JUC-Z4 to heptamolybdate, the system changes from unstable to a stable colloidal regime [Fig. 1(b)]. We observe that dispersions of 3.86×10^{-5} , 7.72×10^{-5} and 1.15×10^{-4} moles of JUC-Z4 give stable dispersions when mixed with 0.1 M and 0.2 M ammonium heptamolybdate based SOMs in 2:1 ratio of volume. The stable dispersion is negatively charge stabilized [Fig. 1(b)].

Now we take the stable dispersion for further characterization and catalytic studies. We first look at the FTIR spectra of the dried SOM-POF dispersion closely and compare it with the peaks of its individual components [Fig. 1(c)]. The fingerprint peaks of ammonium heptamolybdate are retained almost unchanged in the SOM-POF composite. The peak at 1400 cm^{-1} intensifies in the composite as compared to that of ammonium heptamolybdate. This peak is attributed to the bending mode ($\delta_{\text{N-H}}$) of N-H vibration. This intensification is due to the condensation of NH_4^+ counterions around the composite. We also observe shifts in the peaks of JUC-Z4 in the composite. For instance, we observe a shift in the bending mode ($\delta_{\text{C-H}}$) and stretching mode ($\nu_{\text{C-H}}$) of C-H vibration at 845 cm^{-1} and 806 cm^{-1} , respectively in the composite. This indicates that the aromatic C-H bonds of the benzene rings of POF are getting stiffened due to the restriction brought about by the surrounding heptamolybdate clusters. We also observe a slight blue shift in the band around 1123 cm^{-1} . This is attributed to the stretching mode ($\nu_{\text{C-P}}$) of C-P vibration in the SOM-POF composite and occurs due to electron donation from heptamolybdate to positive centre of phosphorous of JUC-Z4 which in turn strengthens the C-P bond.

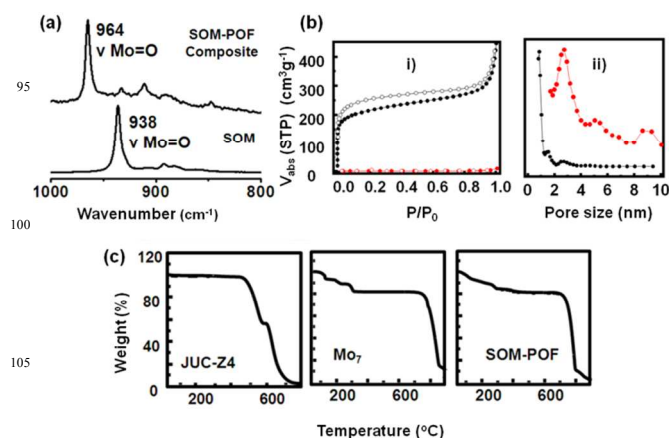


Fig. 2 (a) Raman Spectra of the composite SOM-POF and ammonium heptamolybdate. (b) i) N_2 sorption isotherms of activated JUC-Z4 (black) and SOM-POF (red) (solid symbols, adsorption; open symbols, desorption). ii) Pore size distribution for JUC-Z4 (black) and SOM-POF (red) derived from N_2 adsorption calculated by DFT method. (c) TGA plot of JUC-Z4, Mo_7 (Ammonium heptamolybdate tetrahydrate) and SOM-POF at air condition.

The FTIR spectra of other SOM-POF composites namely SOM-PAF1, SOM-JUC-Z2 and SOM-JUC-Z5 also show characteristic peaks of SOM as well as their respective constituting POF

materials with slight shifts in the peak values indicating successful formation of SOM-POF composites (See SI for details). The loading of PAF-1, JUC-Z2 and JUC-Z5 is varied accordingly and the variation of the zeta potential is studied for obtaining a correspondingly stable SOM-POF composite. (See SI for details).

We now check the Raman spectroscopic signature of the SOM-JUC-Z4 composite and compare it with the dispersion of soft oxometalates. In the Raman spectrum of the composite, there is a shift of the Mo=O peak towards higher wavenumber ($\sim 26 \text{ cm}^{-1}$) [Fig. 2(a)]. This implies successful formation of the SOM-JUC-Z4 composite. This is so because in the composite, the polarizability of the Mo=O bond is much less since it is attached to the electron deficient JUC-Z4, as compared to SOM alone.

The TGA measurements show the decomposition patterns of SOM-POF material as compared to that of the starting materials viz., ammonium heptamolybdate and JUC-Z4 [Fig. 2(c)]. It is observed that the thermal stability of the SOM-POF hybrid is enhanced to 750°C from that of 475°C of JUC-Z4 alone. The same trend is observed for SOM-PAF1, SOM-JUC-Z2 and SOM-JUC-Z5 where the decomposition temperature of each of the composites is increased by $200\text{--}300^\circ\text{C}$ than their POF counterparts (See SI for details). We now test further the capacity of SOM-POF composites for gas adsorption from the BET and Langmuir surface area values and also to see the pore size distribution profile and compare the values with those of the precursor POFs. In order to perform sorption measurements, we make sure that there are no guest molecules such as carbon dioxide, water, oxygen etc. in the SOM-POF material. Such a sample is called the activated sample. To ensure the purity of sample we degas it at 100°C and then perform the N_2 sorption measurements. From the sorption curves [Fig. 2(b)] we calculated the BET and Langmuir surface area of the SOM-JUC-Z4 composite and found it to be $7.49 \text{ m}^2\text{g}^{-1}$ and $10.10 \text{ m}^2\text{g}^{-1}$, respectively. On the other hand, the calculated BET and Langmuir surface area of JUC-Z4 was found to be $793 \text{ m}^2\text{g}^{-1}$ and $979 \text{ m}^2\text{g}^{-1}$, respectively. This means in the case of the composite, the surface area reduces almost 100 times which is attributed to the incorporation of heptamolybdate clusters in the POF pores. The pore size distribution derived from N_2 adsorption calculated by DFT method [Fig. 2(b)] shows the average pore size of the composite to be around 2.73 nm which is inherited from its POF component-JUC-Z4. The 0.93 nm pore of JUC-Z4, however, is not observed in the composite. This indicates that the SOMs block the micropores of the POF whereas the mesopores remain vacant. The existence of these mesopores of 2.73 nm provides the fine hierarchical pore structure which is suitable for catalysis. We also did N_2 adsorption measurements with SOM-PAF1, SOM-JUC-Z2 and SOM-JUC-Z5 composites and determined their BET surface area to be around $9.610 \text{ m}^2\text{g}^{-1}$, $4.928 \text{ m}^2\text{g}^{-1}$ and $14.693 \text{ m}^2\text{g}^{-1}$, respectively. In all these cases it is observed that the surface area is reduced almost 100 fold as in case of SOM-JUC-Z4, implying impregnation of soft-oxometalate units in the POF core-pores (See SI for details).

2. On heterogeneous catalysis by SOM-POF composites:

We now reiterate the question: can simultaneous abundance of phosphorous and molybdenum in a supramolecular structure lead

to the emergence of catalytic behaviour comparable to that of the molecular $[\text{PMo}_{12}]$ Keggin? With this end in view we undertake a model reaction namely oxidation of benzaldehyde to benzoic acid with hydrogen peroxide using the SOM-JUCZ4 dispersion as a catalyst [Fig. 3].

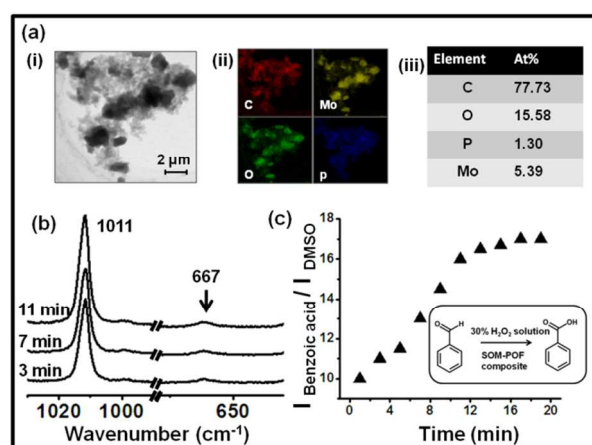


Fig. 3 (a) i) Close up on the SOM-POF composite particle in dispersion. ii) Elemental mapping via EDX-TEM of the SOM-POF dispersion showing various elements present. iii) Table depicting atomic abundance of each element present in the dispersion. (b) Time Resolved Raman Spectroscopic study to show the catalysis of benzaldehyde oxidation using the composite SOM-POF dispersion as catalyst and DMSO as an external standard. (c) $I_{\text{Benzoic acid}}/I_{\text{DMSO}}$ versus time plot indicating increase in intensity of ring breathing mode of benzoic acid (1011 cm^{-1} peak) thereby confirming the catalytic oxidation of benzaldehyde to benzoic acid.

We observe that the SOM-JUC-Z4 dispersion is effective as a catalyst for the oxidation of benzaldehyde in the presence of 30% aqueous hydrogen peroxide using dimethyl sulfoxide (DMSO) as an external standard. We monitor the reaction by time resolved Raman spectroscopy [Fig. 3(b)].

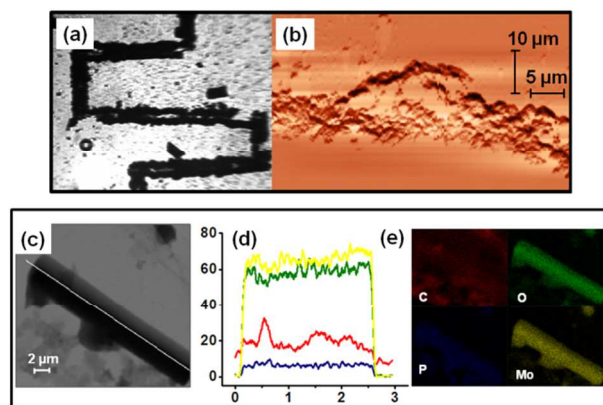


Fig. 4 (a) Close up on the catalytic reactor chip: Trail formation by the composite SOM-POF under the laser of the optical tweezers of 1064 nm wavelength. (b) AFM image showing the topography of the trail. (c) Elemental mapping via line scan of a rod-like structure of SOM-POF composite. (d) Count versus distance plot indicating the abundance of each element namely carbon (red), oxygen (green), phosphorous (blue) and molybdenum (yellow), in the composite catalyst. (e) Elemental mapping of each of the elements shown in (d).

The rate of formation of product benzoic acid increases with time in a sigmoid fashion [Fig. 3(c)] with respect to the added external standard DMSO and shows an initial lag phase of few minutes. Such a presence of lag phase and sigmoidal nature of product formation points to the operation of heterogeneous catalysis as has been shown very nicely in the literature.⁵⁰⁻⁶¹ Indeed in the SOM-JUC-Z4 dispersion we observe composite particles which are a mixture of irregular shaped particles and nanotubes. They possess C, P, Mo and O on a nanoscopic scale in a homogeneous manner as observed from EDX-TEM from the SOM-POF dispersion catalyzing the reaction [Fig. 3(a)].

We speculate these are the active particles that are responsible for the heterogeneous catalysis we observe in the reaction. It is also worth noting the polydispersity in the system as well. In short we speculate that in a heterogeneous catalytic mode these particles of SOM-JUC-Z4 actively catalyze the system. Apart from SOM-JUC-Z4 composite other SOM-POF composites such as SOM-PAF1, SOM-JUC-Z2 and SOM-JUC-Z5 were used to catalyze oxidation of benzaldehyde in presence of hydrogen peroxide as oxidant in dispersion phase. These materials were compared with molecular [PMo₁₂] for their catalytic activity.

3. Catalytic activity of SOM-JUC-Z4 composite, SOM, JUC-Z4 and benchmark molecular [PMo₁₂].

We now compare catalytic activity of SOM, JUC-Z4, SOM-JUC-Z4 composite and [PMo₁₂], our benchmark catalyst. To do so, we study the oxidation of benzaldehyde. The catalytic studies were done by time dependent ¹H NMR studies in dispersion. The reaction mixture comprising of benzaldehyde along with hydrogen peroxide, DMSO (used as an external standard) and SOM-JUC-Z4 composite catalyst were monitored by ¹H NMR at regular time intervals.

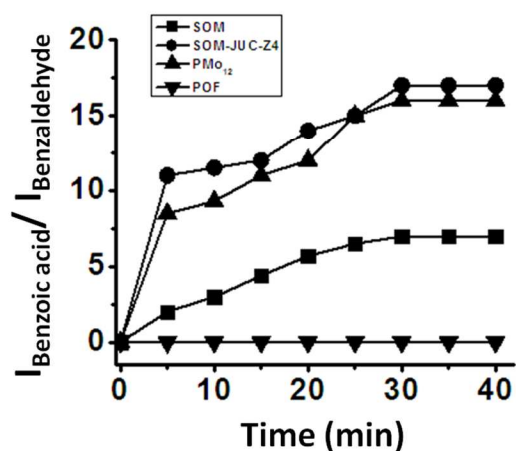


Fig. 5 Plot of ratio of intensity of acidic proton of benzoic acid and aldehydic proton of benzaldehyde versus time using SOM, JUC-Z4, SOM-JUC-Z4 composite and PMo₁₂ obtained by time dependent ¹H NMR studies.

The POF material i.e. JUC-Z4 alone did not show any activity whereas the SOM did show some catalytic activity but it was

quite low as compared to the catalytic activity of the SOM-JUC-Z4 composite [Fig. 5]. This means that the SOM-component in the composite is facilitating the catalysis however its efficiency is amplified in the presence of a porous material with fine accessible mesopores of 2.7 nm which provide the site for catalysis. In fact the supramolecular composite of SOM-JUC-Z4 shows a sort of synergistic effect arising out of SOM and POF and its catalytic activity even surpasses the activity of our benchmark [PMo₁₂] polyoxometalate.

4. Comparative catalytic activity of SOM-POF composites in dispersions and with benchmark [PMo₁₂]

In order to understand the effect of catalyst loading on the yield of benzoic acid, NMR studies were done on dispersions containing the oxidation product i.e. benzoic acid with different loading of different composite catalysts. From the plot between ratio of intensity of acidic proton of benzoic acid peak and intensity of aldehydic proton of benzaldehyde versus amount of catalyst loading, it is observed that SOM-JUC-Z4 showed maximum catalytic activity, even greater than molecular [PMo₁₂] (benchmark catalyst) followed by SOM-JUC-Z5 and almost negligible activity was shown by SOM-PAF1 and SOM-JUC-Z2 [Fig. 6]. Clearly the higher activity of SOM-JUC-Z4 implies the following. 1. The supramolecular composite SOM-JUC-Z4 is an effective catalyst. 2. Since it has mesopores not available in [PMo₁₂], SOM-JUC-Z4 is more efficient than [PMo₁₂], the benchmark catalyst.

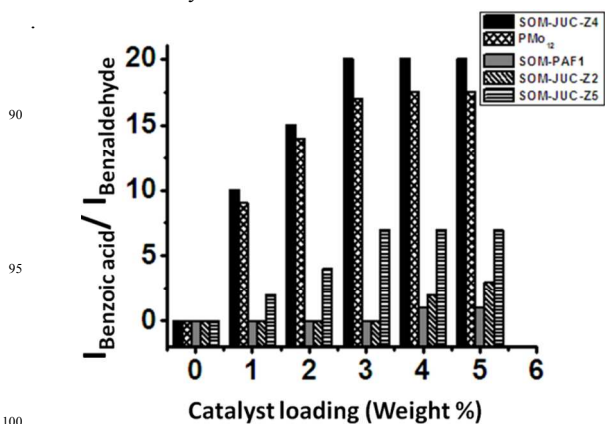


Fig. 6 Plot between ratio of intensity of acidic proton of benzoic acid peak and intensity of aldehydic proton of benzaldehyde peak versus catalyst loading from ¹H NMR studies. The reactions are in dispersions.

5. Comparative kinetic study of aliphatic and aromatic aldehydes oxidation using different SOM-POF composites in dispersion.

Our chosen model reaction system is that of benzaldehyde oxidation with hydrogen peroxide as an oxidant and DMSO as an external standard. This reaction system is used for oxidation using different SOM-POF composites viz., SOM-PAF1, SOM-JUC-Z2, SOM-JUC-Z4, SOM-JUC-Z5 and molecular [PMo₁₂], where [PMo₁₂] is the benchmark catalyst as it is a standard catalyst for oxidation reactions. The kinetics of different reactions is monitored by time dependent ¹H NMR spectroscopy [Fig. 7].

This comparative study showed that SOM-JUC-Z4 has maximum catalytic activity followed by considerable catalytic activity by molecular $[\text{PMo}_{12}]$, SOM-JUC-Z5 and almost no activity by SOM-JUC-Z2 and SOM-PAF1. Such high activity by SOM-JUC-Z4 implies that indeed supramolecular combination of phosphonium and molybdate is as effective in catalysis as elemental P, Mo in $[\text{PMo}_{12}]$. However it is worth noting that SOM-JUC-Z4 composite shows greater catalytic activity than the standard catalyst molecular $[\text{PMo}_{12}]$ which is a known catalyst as well as a catalyst precursor for oxidation reactions [Fig. 7]. Such high activity of SOM-JUC-Z4 compared to $[\text{PMo}_{12}]$ can be attributed to higher accessible mesopores of the composite compared to that of $[\text{PMo}_{12}]$, as mentioned before.

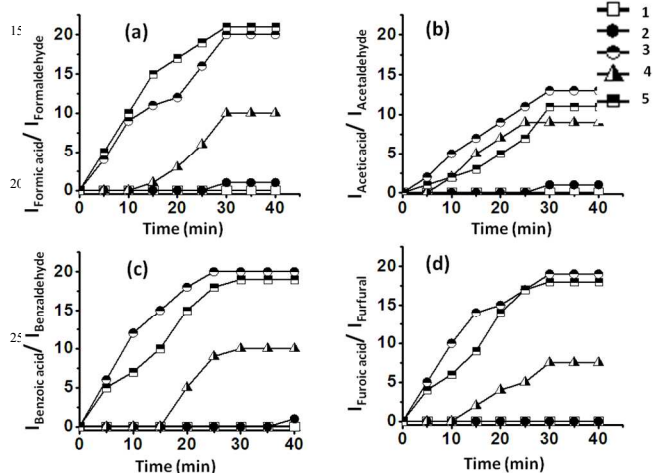


Fig. 7 Plot between ratio of intensity of acidic proton peak of product (i.e. carboxylic acid) and intensity of aldehydic proton peak of reactant (i.e. aldehyde) and time. The results are obtained by time dependent ^1H NMR studies of oxidation of (a) Formaldehyde (b) Acetaldehyde (c) Benzaldehyde (d) Furfural by SOM-POF composites. SOM-POF composites shown in the figure are SOM-PAF1 (1), SOM-JUC-Z2 (2), SOM-JUC-Z4 (3), SOM-JUC-Z5 (4) composites and molecular PMo_{12} (5). The reactions are in dispersions.

6. Optically patterned SOM-POF composite on a chip and its electron microscopic characterization.

Now having shown catalysis by SOM-POF dispersion, we wanted to take the next step. We ask: Can we induce a phase transition and pattern the SOM-POF dispersion and see the effect it has on catalysis in a designed catalytic chip? Can we achieve a site-specific heterogeneous catalysis on such a designed catalytic chip? Now we address these questions.

Recently we have shown that it is possible to write patterns using thermo-optical tweezers starting from a SOM dispersion by inducing soft to crystalline phase transition.¹² Likewise a similar patterning by inducing phase transition in the freshly synthesized SOM-POF dispersion should also be possible. We thus place an aqueous SOM-POF dispersion in our sample holder described earlier. We place this sample holder on a movable scanning stage and then focus 1064 nm laser light on the top surface of the sample holder. The SOM-JUC-Z4 composite has absorptivity of around $105 \text{ mol}^{-1}\text{cm}^{-1}$ at 1064 nm. Hence, the laser light is

absorbed by the composite, so that heating occurs at the focused spot in a localized manner. This, in turn, leads to formation of a water vapour bubble from the water present in the medium. Since in the vicinity of the bubble no such heating has occurred, a temperature gradient is generated which causes convection current. These currents circulate the SOM-POF material and eventually deposit it at the base of the bubble. As the laser beam is translated so that it focuses at a nearby new spot, there can be two possibilities. The first is that a new bubble is generated and the second possibility is that the previously formed bubble migrates to the new spot. Since the latter is thermodynamically more favourable, the initial bubble is also translated to the new location of the laser focus and the chain of events that lead to the deposition of SOM-POF composite continues. In this way we are able to design a catalytic reactor chip comprising patterned trail [Fig. 4(a)] having a width of few micrometres – a fact that is confirmed by the AFM studies [Fig. 4(b)]. TEM measurement of the patterned material is also carried out by scraping off the active catalytic material from the slide.

We now check the elemental composition of the patterned trail and the nature of the active catalytic material. To do so, we re-disperse a part of the catalytic trail in water and drop-cast it on a TEM grid. On subjecting it to elemental mapping we indeed see a molecular level composite of phosphorous and molybdenum to exist in the structures found in the dispersions obtained from the patterned material of SOM-POF. Both elemental mapping and line scan analysis show the presence of phosphorous and molybdenum at atomic level in the structures in the patterned material, thereby proving that we indeed have a composite on a chip whose composition on nanoscopic length scale shows the presence of both phosphorous and molybdenum [Fig. 4(c)-(e)].

7. Catalysis by optically patterned SOM-JUC-Z4 catalyst chip: On heterogeneous catalysis:

Now we test the catalysis of benzaldehyde oxidation by optically patterned SOM-JUC-Z4 composite on the chip. We use the patterned material as a catalyst for benzaldehyde oxidation. We observe by time resolved Raman spectroscopy that the peak intensities of the product, benzoic acid with respect to external standard DMSO increases with time [Fig. 8(a)]. However in addition to general bulk catalysis we checked the possibility of site-specific catalysis on the patterned material surface using dimethyl sulfoxide (DMSO) as an external standard. Here we observe that indeed the reaction is catalysed much more efficiently on the patterned material surface in a site specific fashion. There is also a sigmoidal increase in the formation of product with respect to external standard DMSO ($I_{\text{Benzoic acid}}/I_{\text{DMSO}}$) versus time plot on the trail [Fig. 8(b)]. However this reaction on the trail is more efficient than that of the dispersion, although the nature of catalysis is heterogeneous like that by the dispersion. [Fig. 3(c) & 8(b)] For instance, it is also worth noting that the catalysis by the reactor chip of the patterned surface clearly shows a lag phase of few minutes in the matter of catalysis. [Fig. 8(b)] Such a lag phase coupled with the sigmoidal pattern of kinetics of product formation (benzoic acid) [Fig. 8(b)] clearly points to the operation of a heterogeneous catalysis on the trail surface in this system.⁵⁰⁻⁶¹

We now compare and contrast the catalysis by the trail with the catalysis by the background using DMSO as an external standard. We observe the abundance of unreacted benzaldehyde from the non-patterned background using Raman spectroscopy [Fig. 8(c)-(d)]. This is because after nucleation in the system and formation of the trail there is a lack of active catalyzing particles in the non-patterned background which loses the ability to catalyze the reaction as is obvious from AFM image of the background where no active catalytic particles are present. [Fig. 4(b)].

10

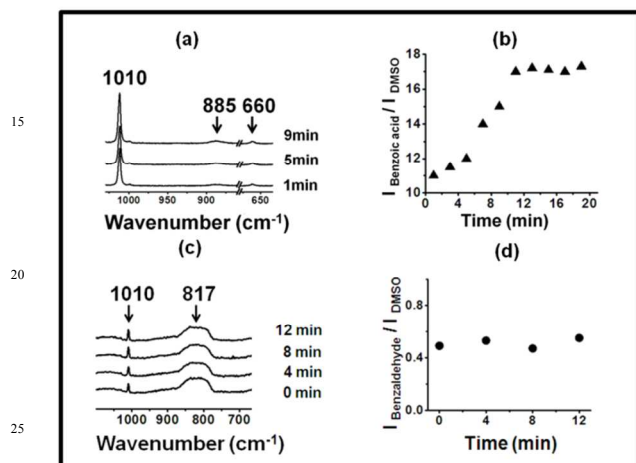


Fig. 8 (a) Time dependent Raman Spectroscopy showing catalysis at trail site. (b) Intensity versus time plot clearly depicting the increase in the intensity of the peak corresponding to the oxidation product, benzoic acid. (c) Time resolved Raman Spectroscopy showing no catalysis away from SOM-POF trail site. (d) Intensity versus time plot clearly depicting the constant intensity of the peak corresponding to the reactant benzaldehyde. Note: DMSO acts as an external standard.

35

These observations have following aspects: 1. The trail is more efficient in catalysis and performs site specific catalysis. 2. The active particles of catalysis are the SOM-POF hybrid particles which are nanotubes and irregular particles in the dispersion and only nanotubes on the crystallized trail. Also note we observe crystallization after laser irradiation from SAED-TEM as we have shown it elsewhere before.¹² 3. Catalysis by both dispersion and the trail is heterogeneous in nature. 4. We can further pin-point that the active species in this catalysis are the rod-shaped SOM-POF nanotubes and irregular particles as seen and characterized in detail by TEM-EDX elemental mapping from the active catalyst trail of the reactor catalyst chip. [Fig. 4(c)-4(e)] Since such particles are not present in the background of the catalytic chip, the background cannot catalyze the reaction [Fig. 7(d)]. Both the sigmoidal kinetics of the reaction and the presence of active particles show that the catalysis in dispersion and on the chip are heterogeneous in nature.

8. Comparison of catalytic activity of various optically patterned SOM-POF composite chips.

The catalytic activity of SOM-JUC-Z4 needs to be compared with other composites in order to do a comparative study of

catalytic activity of SOM-POF materials. To accomplish this, patterned trails of SOM-PAF1, SOM-JUC-Z2 and SOM-JUC-Z5 were designed and these trails were used as sites for benzaldehyde oxidation in presence of hydrogen peroxide as oxidant. Their catalytic activity was compared in terms of ratio of intensity of benzoic acid peak and intensity of DMSO peak (external standard) obtained after the reaction by Raman spectroscopy. We observe that SOM-JUC-Z4 patterned chip is the most effective in catalysis, even more than [PMo₁₂] benchmark [Fig. 9]. This clearly indicates that supramolecular composite of patterned phosphonium with molybdate in SOM-JUC-Z4 is effective in catalysis. Since it has higher mesoscopic accessibility as compared to [PMo₁₂], the SOM-JUC-Z4 patterned chip is more efficient in catalysis.

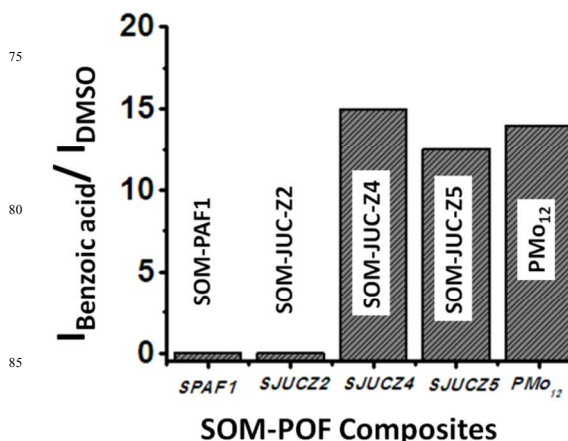


Fig. 9 Catalysis by SOM-POF composite chips: Graph showing ratio of intensity of benzoic acid peak and intensity of DMSO peak from Raman spectroscopy obtained for SOM-PAF1 (SPAF1), SOM-JUC-Z2 (SJUCZ2), SOM-JUC-Z4 (SJUCZ4), SOM-JUC-Z5 (SJUCZ5) composites and molecular [PMo₁₂].

We now place the reaction mixture comprising of benzaldehyde, hydrogen peroxide as an oxidant and DMSO as the external standard on the patterned SOM-POF chip and monitor kinetics of the reaction by Raman spectroscopy [Fig. 10]. The kinetics of all

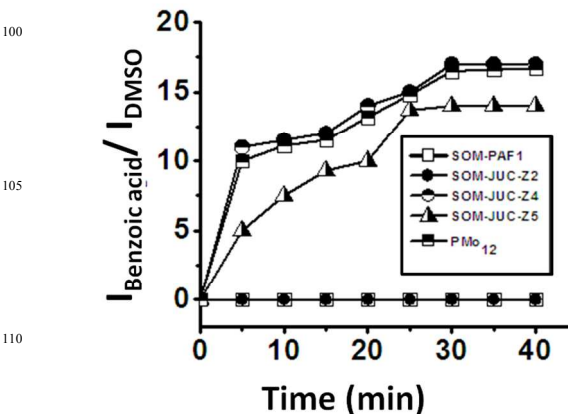


Fig. 10 Kinetics of SOM-POF composite catalyst chip: Plot of ratio of intensity of benzoic acid peak and ratio of intensity of external standard DMSO peak versus time obtained by time dependent Raman studies using different SOM-POF composites and hydrogen peroxide as oxidant.

the patterned chips show sigmoidal behaviour. Catalysis is observed only on the trail and not elsewhere, so it is site-specific. Moreover the patterned trails of SOM-JUC-Z4 shows maximum efficiency as a catalyst for benzaldehyde oxidation followed by the catalytic activity of the trails of molecular $[\text{PMo}_{12}]$ and SOM-JUC-Z5. There is almost no catalytic activity by trails of SOM-JUC-Z2 and SOM-PAF1 [Fig. 10].

9. Stability of the optically patterned catalyst chip

After investigating the catalytic potential of the SOM-JUC-Z4 patterned chip the next step was to see the stability of this catalyst chip. For this purpose the trail was checked for its intactness by Raman spectroscopy post-reaction. It was found that the trail formed by SOM-JUC-Z4 gave the same Raman signatures as it showed before the catalytic reaction thus indicating that the chip is stable and reusable after the reaction [Fig. 11]. The chip is also stable for weeks after its fabrication.

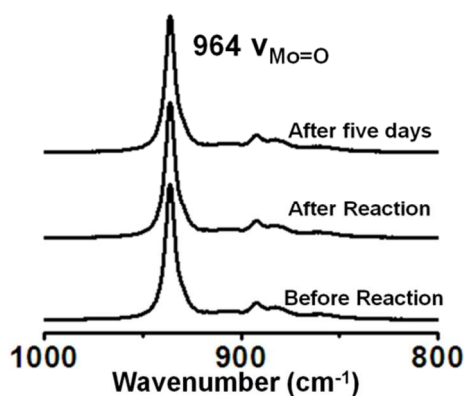


Fig. 11 Raman spectra of SOM-JUC-Z4 composite chip recorded before the reaction, immediately after the reaction and 5 days after the reaction.

10. Comparative kinetic study of aromatic and aliphatic aldehydes oxidation using dispersion and patterned chips of SOM-POF composites as catalysts

The oxidation of different aldehydes viz., formaldehyde, acetaldehyde, furfural and benzaldehyde using all the five catalysts namely SOM-PAF1, SOM-JUC-Z2, SOM-JUCZ-4, SOM-JUC-Z5 and molecular $[\text{PMo}_{12}]$ were studied in dispersion phase in presence of hydrogen peroxide as oxidant. With the aid of time dependent ^1H NMR studies it was found that SOM-JUC-Z4 dispersion showed maximum catalytic activity for the oxidation of all the four aldehydes [Fig. 7]. Among all the aldehydes, the SOM-POF dispersion showed higher selectivity towards oxidation of benzaldehyde followed by formaldehyde, furfural and acetaldehyde, respectively [Fig. 12]. For all the composites, we obtained sigmoidal curves in conversion kinetics which suggest heterogeneous catalysis. SOM-JUC-Z4 patterned chip was then used to catalyze oxidation of aliphatic aldehydes such as formaldehyde, acetaldehyde and aromatic aldehydes namely furfural and benzaldehyde and it was monitored by time dependent Raman spectroscopy. The results obtained from the

patterned catalyst chip were also quite similar to that of the dispersion phase catalysis. The rate of reaction of formaldehyde oxidation was faster than that of furfural followed by acetaldehyde oxidation but the fastest oxidation was that of the benzaldehyde reaction. This implies that the chip formed by SOM-JUC-Z4 composite catalyzes benzaldehyde oxidation at the fastest rate [Fig. 12].

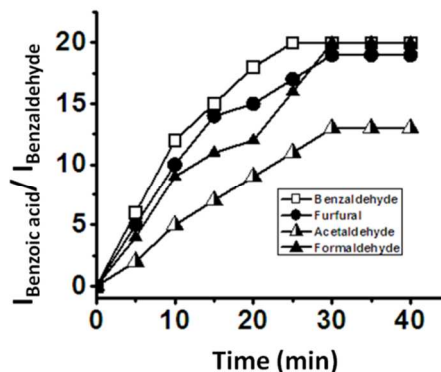


Fig. 12 The ratio of intensity of benzoic acid peak and intensity of benzaldehyde peak versus time plot clearly depicting the catalytic activity of SOM-JUC-Z4 composites in dispersion for oxidation of different aldehydes obtained by time dependent ^1H NMR studies. The reactions are in dispersion.

11. Comparative study of benzaldehyde oxidation using different oxidants.

The effect of different oxidising agents on the rate of reaction was studied by using different oxidants such as hydrogen peroxide, dilute sulphuric acid, dilute nitric acid and silver (I) oxide for oxidation of benzaldehyde in presence of all five catalysts i.e. SOM-PAF1, SOM-JUC-Z2, SOM-JUCZ-4, SOM-JUC-Z5 and molecular $[\text{PMo}_{12}]$. The kinetics of the reactions were monitored by ^1H NMR and the ratio of intensity of acidic proton of benzoic acid peak and intensity of aldehydic proton of benzaldehyde peak was plotted against time. These plots were sigmoidal pointing to the heterogeneous nature of catalysis and

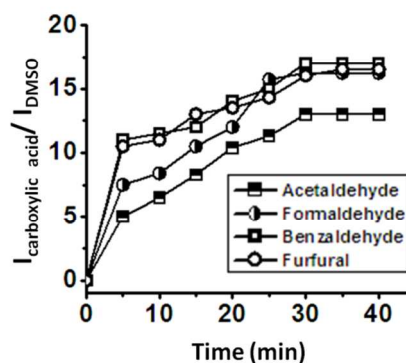


Fig. 13 Catalysis of oxidation of different aldehydes by the SOM-JUC-Z4 patterned catalyst chip: The ratio of intensity of peak of carboxylic acid and intensity of DMSO peak versus time plot clearly depicting the catalytic activity of different SOM-JUC-Z4 composite catalyst chip in oxidation of different aldehydes monitored by time dependent Raman studies.

showed that the highest rate of reaction for benzaldehyde oxidation was with dilute sulphuric acid. Hydrogen peroxide acted as the next efficient oxidant followed by dilute nitric acid and finally silver (I) oxide. (See Supplementary Information for more details) With the maximum product formation obtained in case of SOM-JUC-Z4 catalyst for benzaldehyde oxidation in the dispersion phase, the patterned chip of SOM-JUC-Z4 was chosen to do a comparative study of aldehyde oxidation with the same set of four different oxidising agents, viz., silver (I) oxide, dilute nitric acid, dilute sulphuric acid and hydrogen peroxide. The reactions were monitored by time dependent Raman spectroscopic experiments. It was observed that dilute sulphuric acid acted as the strongest oxidising agent. Hydrogen peroxide and dilute nitric acid showed comparable oxidising ability whereas silver (I) oxide oxidised benzaldehyde to a lesser extent [Fig. 14].

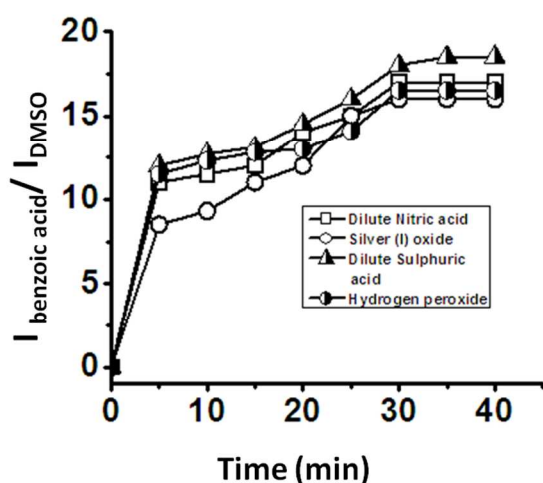


Fig. 14 Kinetics of oxidation by various oxidants on a catalyst chip: Plot of ratio of intensity of the formed benzoic acid peak and ratio of intensity of external standard DMSO peak versus time obtained by time dependent Raman studies using SOM-JUC-Z4 composite as catalyst chip and different oxidants.

Conclusions

To summarize, we have shown that starting from a well defined molecular precursor of a heptamolybdate polyoxometalate, we first synthesized in a controlled way a soft oxomolybdate (SOM) nanotube. This in turn, forms another stable dispersion with a well defined porous aromatic framework namely JUC-Z4.

The composite material is characterized by detailed spectroscopic, gas sorption and microscopy experiments and indeed shows that, in the structure constituting the solid phase of the dispersion, there exist a simultaneous abundance of phosphorous and molybdenum at nano scale.

Hence we test our hypothesis: can this composite act catalytically in a comparable way to that of $[\text{PMo}_{12}]$ Keggin? To do so, we use this composite for catalyzing oxidation of benzaldehyde to benzoic acid using hydrogen peroxide. We observe that not only the dispersion catalyzes the reaction efficiently but also the patterned material comprising of SOM-POF composite. Moreover the catalysis on the surface of SOM-POF patterned material is more pronounced than that of the dispersion. We

further show the operation of heterogeneous mode in catalysis both in the dispersion and on the trail of the chip by observation of sigmoidal kinetics of product formation and by identifying the active catalytic particles. We also show when these particles are not present, as in the background of the catalytic chip, there is no catalysis. A comparative study of different composite materials as dispersions and as chips for oxidation of different aldehydes using different oxidants has been done and based on the kinetic studies we can conclude that SOM-JUC-Z4 composite catalyzes oxidation of benzaldehyde in presence of hydrogen peroxide to the maximum extent even greater than molecular $[\text{PMo}_{12}]$. Such high activity of SOM-JUC-Z4 vindicates two points. 1. Supramolecular composite comprising of phosphonium and molybdate is effective as catalyst. 2. High accessible mesopores of such composite compared to that of molecular $[\text{PMo}_{12}]$ is the reason for its high catalytic activity. This work in turn, implies that it is possible to design a patterned composite material to catalyze deliberately targeted reactions starting from well defined molecular level precursors in a completely controlled fashion.

Acknowledgements

Financial support of DST Fast track, BRNS DAE, India and IISER-Kolkata, India, NSFC grant of P. R. China is gratefully acknowledged. This paper is dedicated to Prof. J.- M. Lehn.

Author contribution: PT synthesized and characterized the SOMs as well as the SOM-POF composites in SR's laboratory. With involvement of SD, PT tested their catalytic activity in dispersion as well as on the chip also in SR's laboratory. CP was instrumental in POF designs, SOM-POF microscopy and porosity measurements at TB's laboratory in SQ's facility. BR and SG were involved in designing the chips along with PT in AB's laboratory. SR initiated the project with TB and AB and coordinated the project and wrote the paper with inputs from PT, AB and TB.

Notes

^a EFAML, Materials Science Centre, Department of Chemical Sciences, IISER-Kolkata, Mohanpur- 741252, India.

*Corresponding author, E-mail: s.roy@iiserkol.ac.in

^b State Key Laboratory of Inorganic Synthesis and Preparative Chemistry, Department of Chemistry, Jilin University, Changchun, People's Republic of China.

*Corresponding author, E-mail: tben@jlu.edu.cn

^c Department of Physical Sciences, Indian Institute of Science Education Research, Kolkata (IISER-Kolkata), Mohanpur- 741252, India.

*Corresponding author, E-mail: qyan@iiserkol.ac.in

References

- W. N. M. Piet. van Leeuwen, *Supramolecular Catalysis*, Wiley-VCH, Weinheim, Germany 2008.
- a) S. Roy, *Comm. Inorg. Chem.* 2011, **32**, 113.
b) S. Roy, *CrystEngComm.* 2014, **16**, 4667–4676.
c) S. Roy (Ed.) *J. Mol. Eng. Mater.* Special Issue on Soft-oxometalates, World Scientific, Singapore, 2014, p. 2.
d) B. Roy, N. Ghosh, S. D. Gupta, S. Roy, A. Banerjee, *N. J. Physics*, 2014 (in press).

- e) S. Das, P. Thomas, S.Roy, *Eur. J. Inorg. Chem.* 2014, DOI: 10.1002/ejic.201402297.
3. A. Ashkin, *Proc. Nat. Acad. Sci. USA* 1997, **94**, 4853-4860.
4. T. Leong, Z. Gu, T. Koh, D. H. Gracias, *J. Am. Chem. Soc.* 2006, **128**, 11336-11337.
5. J. C. Love, A. R. Urbach, M. G. Prentiss, G. M. Whitesides, *J. Am. Chem. Soc.* 2003, **125**, 12696-12697.
6. H. F. Hamann, S. I. Woods, S. Sun, *Nano Lett.* 2003, **3**, 1643-1645.
7. K. G. Yager, C. J. Barrett, *Macromolecules* 2006, **39**, 9320-9326.
8. R. S. Singh, V. Nalla, W. Chen, A. T. S. Wee, W. Ji, *ACS Nano* 2011, **5**, 5969-5975.
9. A. Dzwilewski, T. Wågberg, L. Edman, *J. Am. Chem. Soc.* 2009, **131**, 4006-4011.
10. J. D. Gerding, D. M. Willard, A. V. Orden, *J. Am. Chem. Soc.* 2005, **127**, 1106-1107.
11. W. R. Childs, R. G. Nuzzo, *J. Am. Chem. Soc.* 2002, **124**, 13583-13596.
12. B. Roy, M. Arya, P. Thomas, J. K. Jürgschat, V. Rao, A. Banerjee, C. M. Reddy, S. Roy, *Langmuir* 2013, **29**, 14733-14742.
13. L. D. Zarzar, B. S. Swartzentruber, J. C. Harper, D. R. Dunphy, C. J. Brinker, J. Aizenberg, B. Kaehr, *J. Am. Chem. Soc.* 2012, **134**, 4007-4010.
14. N. M. Andoy, X. Zhou, E. Choudhary, H. Shen, G. Liu, P. Chen, *J Am Chem Soc.* 2013, **135**, 1845-1852.
15. M. T. Pope, *Heteropoly and IsopolyOxometalates*, Springer, Berlin, Germany 1983.
16. A. Müller, S. Roy, in *The Chemistry of Nanomaterials: Synthesis, Properties and Applications*, (Eds: C.N.R.Rao, A. Müller, A.K.Cheetham), Wiley-VCH Verlag GmbH & Co. KGaA, Weinheim, Germany 2005, Ch. 14.
17. a) A. Müller, S. Roy, *Russ. Chem. Rev.* 2002, **71**, 981-991; b) A. A. Verhoeff, M. L. Kistler, A. Bhatt, J. Pigga, J. Groenewold, M. Klokkenburg, S. Veen, S. Roy, T. Liu, W. K. Kegel, *Phys. Rev. Lett.* 2007, **99**, 066104.
18. C. L. Hill, (Ed.) *Chem. Rev.* 1998, **98**, 1-2.
19. M. T. Pope, A. Müller, *Angew. Chem. Int. Ed. Engl.* 1991, **30**, 34.
20. *Inorganic Synthesis*, Vol. 27 (Ed: A. P. Ginsberg), Wiley, New York, USA 1990.
21. C. L. Hill, D. A. Bouchard, *J. Am. Chem. Soc.* 1985, **107**, 5148-5157.
22. *Comprehensive Coordination Chemistry*, (Eds: L. Cronin, J. A. McCleverty, T. J. Meyer), Elsevier, Amsterdam, Netherlands 2004.
23. *Polyoxometalate Chemistry for Nanocomposite Design*, (Eds: T. Yamase, M. T. Pope), Kluwer Academic Publishers, New York, USA 2002.
24. *Introduction to Polyoxometalate Chemistry: From Topology via Self-Assembly to Applications*, (Eds: M. T. Pope, A. Müller), Kluwer Academic Publishers, New York, USA 2001.
25. *Polyoxometalate Molecular Science NATO Science series*, (Eds: J. J. Borra's-Alamemar, E. Coronado, A. Müller, M.T. Pope), Kluwer Academic Publishers, Dordrecht, Netherlands 2003.
26. S. Roy, K. L. Planken, R. Kim, D. v. d. Mandele, W. K. Kegel, *Inorg. Chem.* 2007, **46**, 8469-8471.
27. S. Roy, M. T. Rijneveld-Ockers, J. Groenewold, B. W. M. Kuipers, H. Meeldijk, W. K. Kegel, *Langmuir* 2007, **23**, 5292-5295.
28. S. Roy, H. J. D. Meeldijk, A. V. Petukhov, M. Versluijs, F. Soulimani, *Dalton Trans.* 2008, **21**, 2861-2865.
29. S. Roy, M. C. D. Mourad, M. T. Rijneveld-Ockers, *Langmuir* 2007, **23**, 399-401.
30. S. Roy, L. C. A. M. Bossers, H. J. D. Meeldijk, B. W. M. Kuipers, W. K. Kegel, *Langmuir* 2008, **24**, 666-669.
31. a) A. Proust, R. Thouvenot, P. Gouzerh, *Chem. Commun.* 2008, 1837-1852; b) D. Chen, A. Sahasrabudhe, P. Wang, A. Dasgupta, R. Yuan, S. Roy, *Dalton Trans.* 2013, **42**, 10587-10596.
32. M. E. Davis, *Nature* 2002, **417**, 813-821.
33. D. Farrusseng, *Metal-Organic Frameworks: Applications from Catalysis to Gas Storage*, Wiley-VCH, Weinheim, Germany 2011.
34. T. Ben, S. Qiu, *CrystEngComm.* 2013, **15**, 17-26.
35. S. J. Garibay, *CrystEngComm.* 2013, **15**, 1515-1519.
36. W. Wang, H. Ren, F. Sun, K. Cai, H. Ma, J. Du, H. Zhao, G. Zhu, *Dalton Trans.* 2012, **41**, 3933-3936.
37. K. Konstas, J. W. Taylor, A. W. Thornton, C. M. Doherty, W. X. Lim, T. J. Bastow, D. F. Kennedy, C. D. Wood, B. J. Cox, J. M. Hill, A. J. Hill, M. R. Hill, *Angew. Chem. Int. Ed.* 2012, **51**, 6639-6642.
38. T. Ben, H. Ren, S. Ma, D. Cao, J. Lan, X. Jing, W. Wang, J. Xu, F. Deng, J. M. Simmons, S. Qiu, G. Zhu, *Angew. Chem. Int. Ed.* 2009, **48**, 9457-9460.
39. R. Babarao, S. Dai, D. E. Jiang, *Langmuir* 2011, **27**, 3451-3460.
40. B. Lukose, *J. Phys. Chem. C* 2012, **116**, 22878-22884.
41. A. P. Côté, A. I. Benin, N. W. Ockwig, M. O'Keeffe, A. J. Matzger, O. M. Yaghi, *Science* 2005, **310**, 1166-1170.
42. H. Ren, T. Ben, E. Wang, X. Jing, M. Xue, B. Liu, Y. Cui, S. Qiu, G. Zhu, *Chem. Commun.* 2010, **46**, 291-293.
43. T. Ben, C. Pei, D. Zhang, J. Xu, F. Deng, X. Jing, S. Qiu, *Energy Environ. Sci.* 2011, **4**, 3991-3999.
44. J. Lan, D. Cao, W. Wang, T. Ben, G. Zhu, *J. Phys. Chem. Lett.* 2010, **1**, 978-981.
45. H. Ren, T. Ben, F. Sun, M. Guo, X. Jing, H. Ma, Kun Cai, S. Qiu, G. Zhu, *J. Mater. Chem.* 2011, **21**, 10348-10353.
46. T. Ben, Y. Li, L. Zhu, D. Zhang, D. Cao, Z. Xiang, X. Yao, S. Qiu, *Energy Environ. Sci.* 2012, **5**, 8370-8376.
47. K. A. Kraus, A. E. Marcinkowsky, J. S. Johnson, A. J. Shor, *Science* 1966, **151**, 194-195.
48. a) C. Pei, T. Ben, H. Guo, J. Xu, F. Deng, Z. Xiang, D. Cao, S. Qiu, *Phil. Trans. R. Soc. A* 2013, **371**, 20120312.
b) T. Ben, H. Ren, S. Ma, D. Cao, J. Lan, X. Jing, W. Wang, J. Xu, F. Deng, J. M. Simmons, S. Qiu, G. Zhu, *Angew. Chem.*, 2009, **121**, 9621-9624.
c) C. Pei, T. Ben, Y. Cui, S. Qiu *Adsorption*, 2012, **18**, 375-380.
49. L. C. W. Baker, J. S. Figgis, *J Am Chem Soc.* 1970, **92**, 3794-3797.
50. J.A. Widegren, R.G. Finke, *Journal of Molecular Catalysis A: Chemical* 2003, **198**, 317-341.
51. J. P. Collman, L. S. Hegedus, J. R. Norton, R. G. Finke, *Principles and Applications of Organotransition Metal Chemistry*, University Science Books, Mill Valley, 1987 (Chapter 10).
52. G. M. Whitesides, M. Hackett, R. L. Brainard, J. P. P. M Lavalleye, A. F. Sowinski, A. N. Izumi, S. S. Moore, D.W. Brown, E. M. Staudt, *Organometallics* 1985, **4**, 1819-1830.
53. Y. Lin, R. G. Finke, *Inorg. Chem.* 1994, **33**, 4891-4910.
54. K. S. Weddle, J. D. Aiken III, R. G. Finke, *J. Am. Chem. Soc.* 1998, **120**, 5653-5666.
55. J. A. Widegren, M. A. Bennett, R. G. Finke, *J. Am. Chem. Soc.* 2003, **125**, 10301-10310.
56. M. A. Watzky, R. G. Finke, *J. Am. Chem. Soc.* 1997, **119**, 10382- 10400.
57. J. A. Widegren, J. D. Aiken III, S. Özkar, R. G. Finke, *Chem. Mater.* 2001, **13**, 312-324.
58. Y. Lin, R.G. Finke, *J. Am. Chem. Soc.* 1994, **116**, 8335-8353.
59. J. D. Aiken III, R. G. Finke, *Chem. Mater.* 1999, **11**, 1035-1047.
60. S. Özkar, R.G. Finke, *J. Am. Chem. Soc.* 2002, **124**, 5796-5810.
61. V. Artero, M. Fontecave, *Chem.Soc.Rev.*, 2013, **42**, 2338-2356.

Table of contents

5

